JOURNAL OF Materials CHEMISTRY

High-surface-area zeolitic silica with mesoporosity

Huanting Wang, Zhengbao Wang, Limin Huang, Anupam Mitra, Brett Holmberg and Yushan Yan*

Department of Chemical and Environmental Engineering, University of California, Riverside, CA 92521, USA. E-mail: Yushan.Yan@ucr.edu

Received 8th March 2001, Accepted 1st June 2001
First published as an Advance Article on the web 30th July 2001

In this study, we report a new, simple approach to the preparation of high-surface-area zeolitic silica (HZS) with well-defined mesoporosity by combining hydrothermal synthesis and sol–gel processing. N_2 adsorption–desorption measurements show that HZS has a BET surface area of 678–723 $m^2\ g^{-1}$ and well-defined bimodal pores at 5.5 and 26.0–34.5 Å. XRD, TEM and FT-IR show that HZS has a typical zeolite MFI structure. HZS is thermally stable and has tunable pore size and pore volume, and thus is promising for applications in catalysis, separation, and microelectronics. The described approach also appears general and may be readily extended to zeolitic aluminosilicates by using suspensions of other zeolite nanoparticles.

1 Introduction

Silicas with uniform micro- or meso-pore structures have attracted much attention because of their demonstrated and projected applications in catalysis and separation.[1–4] Application of micro- and meso-porous silicas as low *k* inter-metal dielectrics in microelectronic devices has also been proposed and studied recently.[5–8] Mesoporous silicas are mostly synthesized by using either long-chain surfactants or block copolymers as the template.[3,4,9] Although mesoporous silicas have highly ordered large pores, their pore walls are amorphous, leading to relatively low thermal/hydrothermal stability.[3,4] Introduction of aluminium (or transition metals) into mesoporous silica through direct synthesis to give strong zeolite-type acidity has not proved straightforward. Also, application of mesoporous silicas in shape-selective catalysis and molecular sieving separation as originally envisioned are yet to be demonstrated. By contrast, microporous zeolites are highly crystalline with well-established use in shape-selective catalysis and molecular sieving separation.[1] They can also have strong acidity and good thermal/hydrothermal stability. However, relatively slow mass transport through their small micropores has been a concern. Clearly, a hierarchical porous material that combines advantages of both microporous crystalline zeolites and mesoporous silicas is desirable. Thus far, however, success in this area has been limited. For example, polystyrene beads were recently used as a second template in a dual template approach to generate macroporosity in zeolitic silica.[10] Using a similar strategy, a mesoporous zeolite was prepared using carbon nanoparticles as the filler;[11] however, the mesoporosity so generated had a rather wide pore size distribution. We have recently demonstrated that zeolitic silica with well-defined meso- or macroporosity can be obtained by self-assembly of monodisperse silicalite nanocrystals.[12] We have also demonstrated that the mechanical strength of the assembled monolithic structures from monodisperse zeolite nanocrystals such as a spin-on film can be significantly improved by a secondary growth treatment.[13,14] In this study, we report another new approach that leads to high-surface-area zeolitic silica with controlled mesoporosity (HZS) by direct gelation of an as-synthesized colloidal suspension of silicalite nanoparticles. We also provide detailed characterization of the material using nitrogen adsorption–desorption, X-ray diffraction (XRD), infrared spectroscopy (IR), transmission electron microscopy (TEM), thermogravimetric analysis (TGA), and scanning electron microscopy (SEM). Because of the presence of low molecular weight silicate species and zeolitic nanoparticles with a range of particle sizes in the as-synthesized suspension,[15–17] the resultant materials can be easily sintered and are mechanically strong. We consider the described approach useful for forming monolithic porous structures for separation, catalysis, and microelectronic devices. For example, we have used this approach to fabricate porous silica films on silicon wafers by a spin-on process, and the resultant film has a low dielectric constant and good adhesion and mechanical strength.[18]

2 Experimental

2.1 Preparation of high-surface-area zeolitic silica with mesoporosity (HZS)

The colloidal suspension of zeolitic nanoparticles was synthesized hydrothermally using an aqueous clear solution.[12,19] The solution was typically prepared by dropwise addition of tetrapropylammonium hydroxide solution (TPAOH, 40 wt%, SACHEM) into TEOS (98%, Aldrich) with strong agitation followed by 3 days of aging at 30 °C under stirring. The molar composition of the final solution was 1 TPAOH : 2.8 SiO_2 : 11.2 EtOH : 40 H_2O. To obtain a stable colloidal suspension of zeolitic particles, the synthesis solution was crystallized at 80 °C for 3 days with constant stirring at 250 rpm in a close-capped polypropylene bottle. Then the milky colloidal suspension was cooled to room temperature under stirring. Zeolitic silica with controlled mesoporosity was prepared by simple drying of the nanoparticle suspension at room temperature or at 80 °C overnight (denoted as HZS-1 and HZS-2, respectively). Samples were calcined at 500 °C for 12 h before characterization.

2.2 Characterization

Nitrogen adsorption–desorption measurements were carried out at −196 °C on a Micromeritics ASAP 2010 instrument to determine the Brunaer–Emmett–Teller (BET) surface area of HZS, and to estimate the pore size distribution using Barrett–Joyner–Halenda (BJH) and Horvath–Kawazoe (HK) calculation procedures for mesopores and micropores, respectively.[20] Before measurement, samples were evacuated overnight at

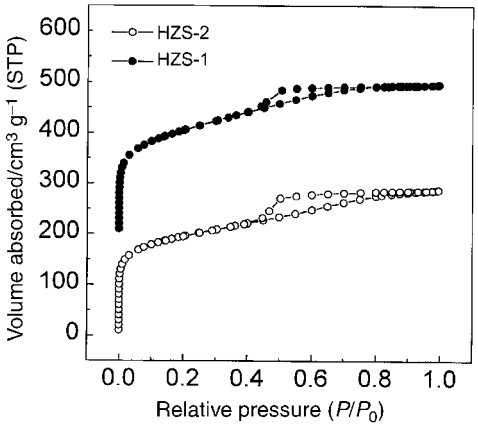

Fig. 1 Nitrogen adsorption–desorption isotherms of HZS-1 and HZS-2 calcined at 500 °C for 12 h. The isotherms are offset by 200 $cm^3\ g^{-1}$ for clarity.

350 °C and 1 μmHg. The total pore volume, V_{total}, was taken from the desorption branch of the isotherm at $P_i/P_0 = 0.98$ assuming complete pore saturation. The volume of micropores, V_{micro}, was determined by the *t*-plot method. The volume of mesopores, V_{meso}, was estimated from the equation: $V_{meso} = V_{total} - V_{micro}$. Thermal decomposition of the organic structure-directing agent (TPAOH in this case) was monitored by thermogravimetric (TG, Cahn D-200) analysis at a heating rate of 5 °C min^{-1} in air. As-synthesized HZS samples were dried at 100 °C for 24 h before TG analysis. X-Ray diffraction (XRD, Siemens D-500 diffractometer using Cu Kα radiation) was employed to identify crystalline phases present in HZS samples. Samples calcined at different temperatures were examined with a scanning electron microscope (SEM, Philips XL30-FEG at 20 kV) and a transmission electron microscope (TEM, Philips CM 300 at 200 kV). Fourier transform infrared (FT-IR, Bruker Equinox 55) spectra were used to analyze sample structures (0.5 cm^{-1} resolution).

3 Results and discussion

3.1 BET surface area and pore size distribution

N_2 adsorption–desorption isotherms of HZS-1 and HZS-2 are shown in Fig. 1. The adsorption steps at low relative pressures signify the filling of the micropores, and hysteresis loops at higher relative pressures show the presence of mesopores. The pore size distributions in Fig. 2 clearly show that both HZS-1 and HZS-2 have a well-defined bimodal pore size distribution. The micropore size is about 5.5 Å, which is characteristic of silicalite. A more detailed analysis of N_2 adsorption–desorption isotherms is summarized in Table 1. The samples have a BET surface area of *ca.* 678–723 $m^2\ g^{-1}$. The micropore volume of the samples is 0.14–0.15 $cm^3\ g^{-1}$, which is lower than that of pure silicalite nanocrystals (*ca.* 0.19–0.20 $cm^3\ g^{-1}$), indicating the presence of amorphous material in the sample. It has been shown that silicalite nanocrystals form by aggregation of nanoslabs ($1.3 \times 4 \times 4$ nm) from TPAOH-directed hydrolysis of TEOS.[15–17] Therefore it is reasonable to expect the as-synthesized suspension to consist of nanocrystals, nanoslabs, and low molecular weight silicate species from TEOS hydrolysis. Clearly, the final material obtained by direct

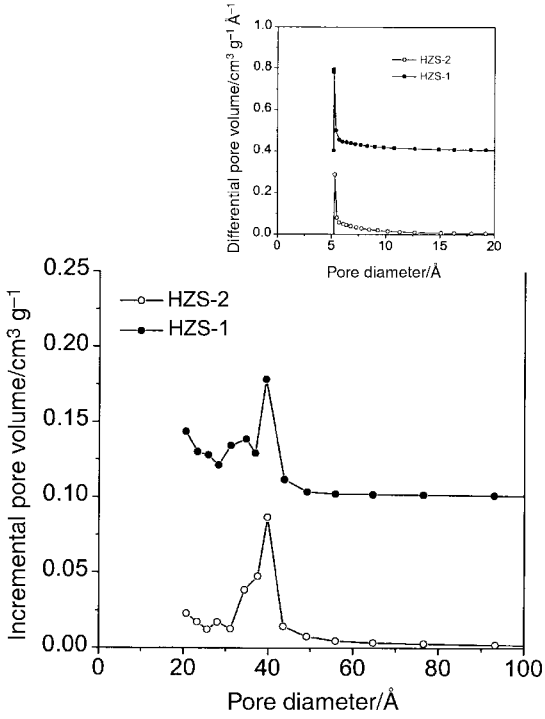

Fig. 2 Mesopore size distribution of HZS-1 and HZS-2 calcined at 500 °C for 12 h calculated by the BJH method. Incremental pore volume is offset by 0.1 $cm^3\ g^{-1}$ for clarity. Inset: micropore size distribution calculated by the HK method. Differential pore volume is offset by 0.4 $cm^3\ g^{-1}\ Å^{-1}$ for clarity.

gellation of the as-synthesized suspension would include contributions from nanocrystals, nanoslabs, and amorphous silica gel from silicate species. The presence of amorphous silica gel explains the observed low micropore volume. The mesopore volume varies from 0.29 to 0.31 $m^3\ g^{-1}$ due to change of packing density of the nanoparticles at different drying temperatures (*e.g.* ambient for HZS-1 *vs.* 80 °C for HZS-2). It is also noted that the mesopore size here is much smaller than that (17 nm) of hierarchical porous material self-assembled from *monodisperse* silicalite nanocrystals[12] because of the presence of nanoslabs and silica gel.

3.2 Crystallinity

XRD, TEM, and FT-IR were performed on both HZS-1 and HZS-2 materials and similar results are obtained. Here we present only the results on HZS-2 as an example. The XRD pattern of HZS-2 shows that HZS has a typical MFI structure (Fig. 3). TEM confirms the presence of highly crystalline nanocrystals in the size range of 25–50 nm (Fig. 4). The FT-IR spectrum shows typical Si–O–Si framework bands including the characteristic double ring vibration at *ca.* 550 cm^{-1} and a shoulder at 980 cm^{-1} attributable to Q^3 Si–OH groups (Fig. 5).[19] The crystallinity is estimated to be 80% from the IR optical density ratio of bands of 550 to 450 cm^{-1}, again confirming the presence of amorphous materials.[21]

TGA and DTG curves of HZS-1 are shown in Fig. 6. TGA gives a total weight loss of 30%. At $T < 170$ °C, there is a weight loss of *ca.* 2% due to desorption of water and external surface

Table 1 N_2 adsorption–desorption results of samples HZS-1 and HZS-2 both calcined at 500 °C for 12 h

Sample	BET surface area/$m^2\ g^{-1}$	Micropore volume/$cm^3\ g^{-1}$	Micropore surface area/$m^2\ g^{-1}$	Mesopore diameter/Å	Mesopore pore volume/$cm^3\ g^{-1}$	Mesopore surface area/$m^2\ g^{-1}$	Total pore volume (at $P/P_0 = 0.98$)/$cm^3\ g^{-1}$
HSZ-1	723	0.14	233	31.0	0.31	490	0.45
HZS-2	678	0.15	318	34.5	0.29	360	0.44

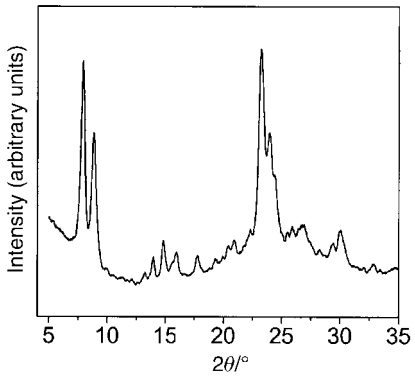

Fig. 3 XRD pattern of HZS-2 calcined at 500 °C for 12 h.

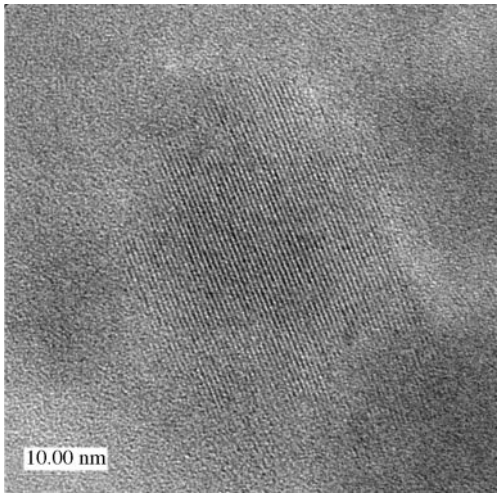

Fig. 4 TEM image of HZS-2 calcined at 500 °C for 12 h.

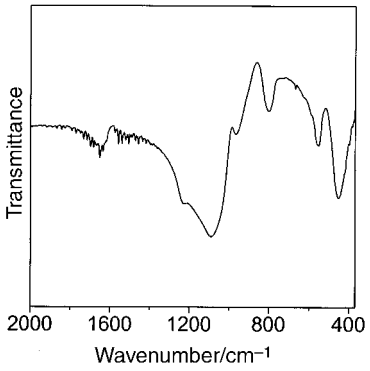

Fig. 5 FT-IR spectrum of HZS-2 calcined at 500 °C for 12 h.

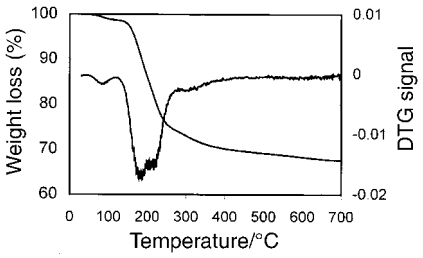

Fig. 6 TGA and DTG curves of HZS-1 dried at 100 °C for 24 h.

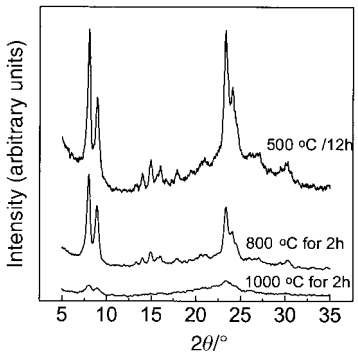

Fig. 7 XRD patterns of HZS-2 calcined under different conditions.

adsorbed TPA molecules. At $T > 170$ °C, there is a weight loss of 28%, and this is attributed to the decomposition of occluded TPA molecules. The weight loss of 28% is greater than the theoretical value of 11.7 wt% assuming four TPA^+ cations per unit cell in a pure silicalite crystal,[15] clearly suggesting that there are additional TPA molecules trapped within the dried silica. It is likely that these TPA molecules reside in the mesopores. From DTG curves, two peaks are observed at 170–220 °C. It is possible that the lower peak is associated with decomposition of TPA in mesopores and the higher one for that of TPA in micropores. Both peaks appear at a temperature which is lower than the typical decomposition temperature of TPA in pure micrometer-sized silicalite crystals, suggesting that TPA molecules located in small nanocrystals decompose more easily than those in large silicalite crystals.

3.3 Thermal stability

The thermal stability of HZS-1 and HZS-2 was studied by calcination at different temperatures, and similar results are obtained. Again, results on HZS-2 are presented as an example. XRD patterns of HZS-2 calcined at 500, 800, and 1000 °C are shown in Fig. 7. There is a slight decrease of peak intensity when the calcination temperature is increased from 500 to 800 °C. When the calcination temperature is raised to 1000 °C, however, the peaks become very weak indicating that HZS-2 loses its crystallinity. N_2 adsorption–desorption isotherms of HZS-2 calcined at different temperatures are shown in Fig. 8 and detailed analysis of the isotherms is summarized in Table 2. The micropore volume of HZS-2 decreases moderately when the calcination temperature is increased from 500 to 800 °C, but it drops by a factor of 3.5 when the calcination temperature is increased to 1000 °C. The BET surface area and mesopore volume follow similar trends. These results agree well with XRD observations. It is noted here that pure monodisperse silicalite nanocrystals with a nominal particle size of 80 nm are very stable at 1000 °C. The decrease of pore volume and surface

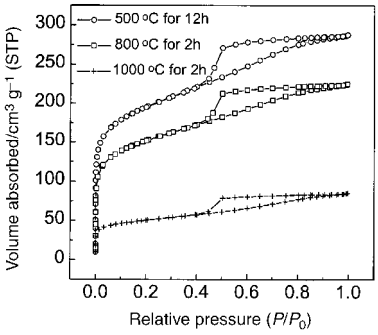

Fig. 8 Nitrogen adsorption–desorption isotherms of HZS-2 calcined under different conditions.

Table 2 Effects of calcination conditions upon the pore structure of HZS-2

Calcination conditions /temperature (°C)/time (h)	BET surface area/$m^2\ g^{-1}$	Micropore volume/$cm^3\ g^{-1}$	Micropore surface area/$m^2\ g^{-1}$	Mesopore diameter/Å	Mesopore pore volume/$cm^3\ g^{-1}$	Mesopore surface area/$m^2\ g^{-1}$	Total pore volume (at $P/P_0 = 0.98$)/$cm^3\ g^{-1}$
500/12	678	0.15	318	34.5	0.29	360	0.44
800/2	528	0.11	240	34.1	0.24	288	0.36
800/12	477	0.09	194	34.2	0.24	282	0.33
1000/2	175	0.04	82	37.5	0.09	93	0.13

area of HZS-2 at high temperature is likely due to structural collapse of small particles (*e.g.* nanoslab and silica gel particles). This is further supported by SEM observation, where images show that HZS-2 samples calcined at different temperatures have similar morphologies, suggesting that well-defined nanocrystals can survive calcination at high temperatures (Fig. 9).

Mesopore size and volume of HZS obtained using the described method can be tuned simply by controlling the synthesis conditions. For example, extra ethanol was added to the clear silicate synthesis solution to form a final composition of 1 TPAOH : 2.8 SiO_2 : 22.4 EtOH : 40 H_2O, and the resulting clear solution was treated through the same hydrothermal and sol–gel procedure. N_2 adsorption–desorption measurements reveal that the resultant HZS has a BET surface area of 684 $m^2\ g^{-1}$, a micropore volume of 0.14 $cm^3\ g^{-1}$, a mesopore volume of 0.13 $cm^3\ g^{-1}$, and a mesopore diameter of 26.0 Å when the sample was dried at ambient temperature. Clearly the mesopore volume and diameter have been reduced (relative to HZS-1 and HZS-2). It is known that ethanol is a by-product of TEOS hydrolysis, and addition of ethanol in the synthesis solution tends to slow down the silicalite crystallization process and helps produce small and uniform nanocrystals.[22] Because of the lower conversion, it is also expected that the as-synthesized suspension contains more low-molecular-weight silicate species. Therefore the observed decrease in mesopore volume and pore diameter is reasonable.

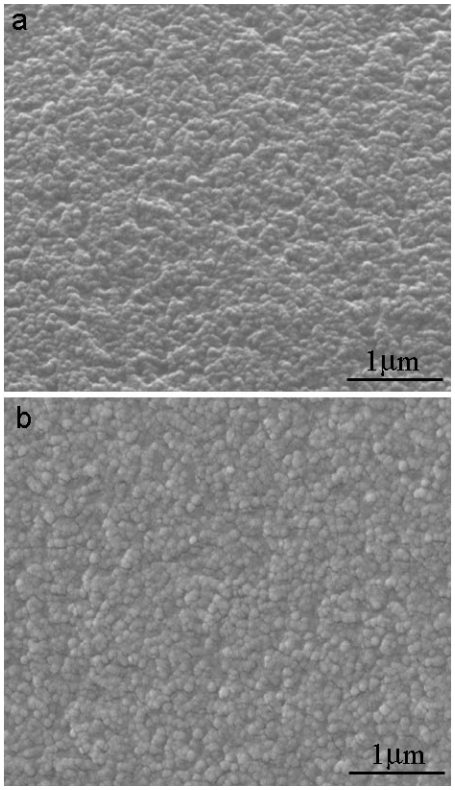

Fig. 9 SEM images of HZS-2 calcined under different conditions: (a) at 500 °C for 12 h, (b) at 1000 °C for 2 h.

Conclusions

High-surface-area zeolitic silica with well-defined mesopores has been prepared simply from a colloidal suspension of silicalite naoparticles and low-molecular-weight silicate species. N_2 adsorption–desorption measurements show that HZS has a BET surface area of 678–723 $m^2\ g^{-1}$, a sharp micropore at 5.5 Å, and a narrow mesopore at 26.0–34.5 Å. HZS has good thermal stability because of its partial crystalline structure. The mesopore size and volume of HZS can be readily adjusted by modifying the synthesis conditions of the colloidal suspension and the drying and sintering conditions. The approach of combined hydrothermal synthesis and sol–gel processing as demonstrated here provides a new route to monolithic crystalline silica (*e.g.* thin films) with hierarchical porosity.

Acknowledgements

Financial support from UC-SMART, Honeywell International, US-EPA, UC-TSR&TP, UC-EI and CE-CERT are gratefully acknowledged.

References

1 S. I. Zones and M. E. Davis, *Curr. Opin. Solid State Mater. Sci.*, 1996, **1**, 107.
2 C. T. Kresge, M. E. Leonowicz, W. J. Roth, J. C. Vartuli and J. S. Beck, *Nature*, 1992, **359**, 710.
3 N. K. Raman, M. T. Anderson and C. J. Brinker, *Chem. Mater.*, 1996, **8**, 1682.
4 J. Y. Ying, C. P. Mehbert and M. S. Wong, *Angew. Chem., Int. Ed.*, 1999, **38**, 56.
5 Z. B. Wang, H. T. Wang, A. Mitra, L. M. Huang and Y. Yan, *Adv. Mater.*, 2001, **13**, 746.
6 D. Y. Zhao, P. D. Yang, N. Melosh, J. L. Feng, B. F. Chmelka and G. D. Stucky, *Adv. Mater.*, 1998, **10**, 1380.
7 Y. F. Lu, H. Y. Fan, N. Doke, D. A. Loy, R. A. Assink, D. A. LaVan and C. J. Brinker, *J. Am. Chem. Soc.*, 2000, **122**, 5258.
8 S. Baskaran, J. Liu, K. Domansky, N. Kohler, X. L. Li, C. Coyle, G. E. Fryxell, S. Thevthasan and R. E. Williford, *Adv. Mater.*, 2000, **12**, 291.
9 D. Y. Zhao, J. L. Feng, Q. S. Huo, N. Melsoh, G. H. Fredrickson, B. F. Chmelka and G. D. Stucky, *Science*, 1998, **279**, 548.
10 B. T. Holland, L. Abrams and A. Stein, *J. Am. Chem. Soc.*, 1999, **121**, 4308.
11 C. J. H. Jacobsen, C. Madsen, J. Houzvicka, I. Schmidt and A. Carlsson, *J. Am. Chem. Soc.*, 2000, **122**, 7116.
12 L. M. Huang, Z. B. Wang, J. Y. Sun, L. Miao, Q. Z. Li, Y. S. Yan and D. Y. Zhao, *J. Am. Chem. Soc.*, 2000, **122**, 3530.
13 Z. B. Wang, H. T. Wang, A. Mitra, L. M. Huang and Y. Yan, *Stud. Surf. Sci. Catal.* 2001, **135**, in press.
14 A. Gouzinis and M. Tsapatsis, *Chem. Mater.*, 1998, **10**, 2497.
15 C. E. A. Kirschhock, R. Ravishankar, P. A. Jacobs and J. A. Martens, *J. Phys. Chem. B*, 1999, **103**, 11021.
16 C. E. A. Kirschhock, R. Ravishanker, L. V. Looveren, P. A. Jacobs and J. A. Martens, *J. Phys. Chem. B*, 1999, **103**, 4972.
17 C. E. A. Kirschhock, R. Ravishanker, F. Verspeurt, P. J. Grobet, P. A. Jacobs and J. A. Martens, *J. Phys. Chem. B*, 1999, **103**, 4965.
18 Z. B. Wang, A. Mitra, H. T. Wang, L. M. Huang and Y. Yan, *Adv. Mater.* 2001, in press.
19 H. T. Wang, Z. B. Wang and Y. S. Yan, *Chem. Commun.*, 2000, 2333.
20 S. J. Gregg and K. S. W. Sing, *Adsorption, Surface Area and Porosity*, Academic Press, London, 2nd edn., 1982.
21 G. Coudurier, C. Naccache and J. C. Vedrine, *J. Chem. Soc., Chem. Commun.*, 1982, 1413.
22 A. E. Persson, B. J. Schoeman, J. Sterte and J. E. Otterstedt, *Zeolites*, 1994, **14**, 557.